

Features of Phase Formation and Phase Distribution in the Dehydration of Coarse Gibbsite Floccules

S. R. Egorova and A. A. Lamberov

Kazan (Volga) Federal University, ul. Kremlevskaya 18, Kazan, Tatarstan, 420008 Russia
e-mail: segorova@rambler.ru

Received June 30, 2014

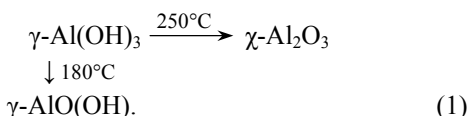
Abstract—A complex study of the phase composition and phase distribution in coarse floccules of the dehydration products of gibbsite thermally treated at atmospheric pressure in air at 250–500°C was performed. The dehydration of gibbsite floccules generates coarsely and finely crystalline boehmite phases. Finely crystalline boehmite is formed by partial “fragmentation” of gibbsite crystals. The layer of coarse boehmite crystals surrounds a finely crystalline boehmite core. $\chi\text{-Al}_2\text{O}_3$ predominantly crystallizes on the outer surface of gibbsite particles that contacts with the environment.

Keywords: gibbsite, boehmite, dehydration, alumina, floccule

DOI: 10.1134/S1070363214120020

Phase transformations of aluminum trihydroxides, in particular, gibbsite, have been studied for a long time [1]. The regularities of phase formation on thermal treatment of gibbsite in air have been the subject of much research [2–9]. Major pathways of phase transitions in gibbsite both at low [7–12] and high (for a few minutes) [3–5] heating rates were established.

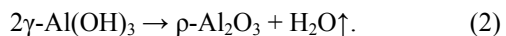
Under near-equilibrium conditions, when dehydration and transformation of crystal lattice occur simultaneously, the thermal decomposition of gibbsite particles more than 1 μm in diameter under heating in air follows two parallel pathways forming boehmite and $\chi\text{-Al}_2\text{O}_3$ [13].



Boehmite formation is initiated at temperatures above 180°C, which is explained by hindered diffusion of water released inside coarse gibbsite particles, as a result of which hydrothermal conditions develop [13]. The formation of boehmite destroys gibbsite layers along the lines passing through holes in the hexangular network [14]. Therewith, zigzag chained aluminum–oxygen octahedra with OH groups at vertices are formed and further dehydrated to form boehmite

double aluminum oxide layers. By contrast, to form crystalline $\chi\text{-Al}_2\text{O}_3$ removal is required of the released water from the reaction zone. Therefore, theoretically, the process in crystals less than 1 μm in diameter can be initiated only after coarse gibbsite particles have been destroyed along the contact plane to form open pores. However, really, this process takes place only at $\geq 250^\circ\text{C}$ [13, 15], to form densely packed oxide aluminum–oxygen layers, the OH[−] layers in $\gamma\text{-Al(OH)}_3$ should get closer to each other, which requires additional energy [16].

At high heating rates during thermochemical and centrifugal thermal activation [3–5] gibbsite converts into an X-ray amorphous product by reaction (2) [2, 17]. Thus product is structurally similar to its precursor, it is thermally stable up to 800°C and shows enhanced reactivity.



At present there is no unambiguous opinion which is the limiting stage of boehmite formation. According to Brown et al. [18], the process is controlled by water diffusion in gibbsite crystals and water desorption; in [19–21] it is suggested that the limiting stage involves the formation and/or growth of nuclei of a new phase (boehmite). The activation energies of the process reported by different authors vary over a wide range (from 14 to 313 kJ/mol) [12, 19–23], which is due to

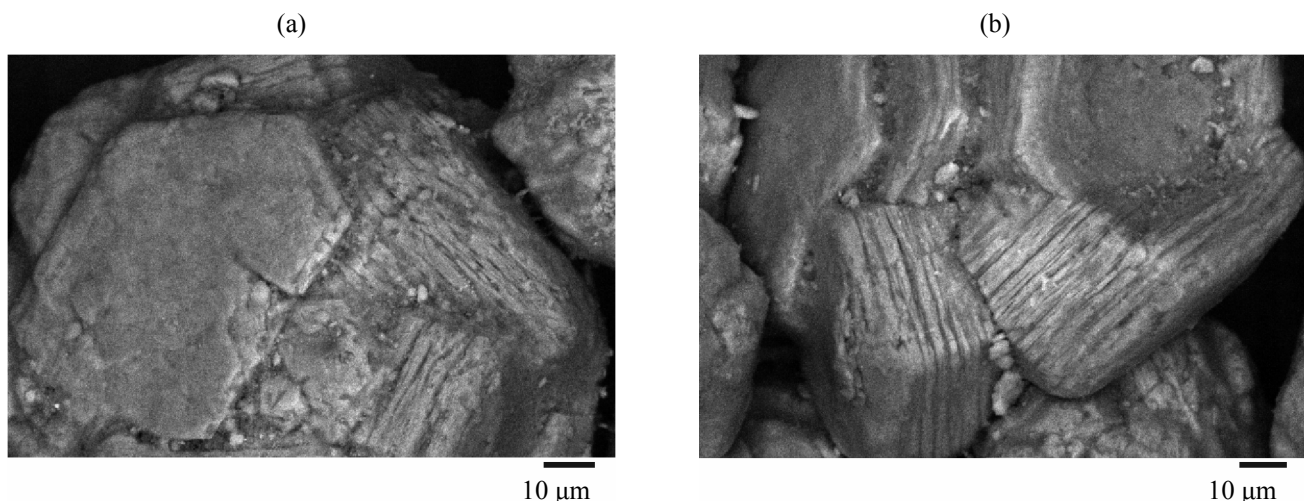


Fig. 1. SEM images of gibbsite samples: (a) starting and (b) thermally treated at 300°C for 300 min.

the different conditions of thermal treatment and procedures for evaluation of phase content used in these works. For example, the activation energy of 272 ± 12 kJ/mol reported by Stacey [22] was determined for a fluidized-bed process under helium and the partial pressure of saturated water vapor of 160–2660 Pa. Madarasz et al. [19] estimated the activation energies for gibbsite amorphization and boehmite nucleus formation (14 ± 1 and 44 ± 3 kJ/mol, respectively) under short (0.5–13 min) isothermal treatment of gibbsite floccules at 550–650°C.

The information on the character of boehmite and $\gamma\text{-Al}_2\text{O}_3$ phase distribution during thermal decomposition of coarse gibbsite particles (primarily in the bulk or on the outer surface) is also quite scarce. Stacey [22] used electron microscopy to show that the dehydration of gibbsite under a low pressure of water vapor can provide boehmite particles up to 100 nm in size in the bulk of decomposing gibbsite, which constitutes an amorphous alumina scaffold.

It seems urgent to gain further insight into the mechanisms and activation energies of boehmite and alumina nucleation, as well as phase localization in the bulk of coarse gibbsite particles. The products of thermal decomposition of gibbsite in the form of micron floccules have found wide use as precursors of aluminum oxide carriers (or carriers proper) for catalysts in a number of petrochemical processes in fluidized-bed reactors [25, 26]. The size of synthetic gibbsite floccules vary from 0.1 to 500 μm and depend on crystallization conditions [26]. This makes it possible to obtain floccules of a desired size and

synthesize on their basis fluidized-bed catalysis. The gibbsite floccules as an alumina carrier are applied due to their small specific surface area ($<1 \text{ m}^2/\text{g}$).

Alumina catalyst carriers or their precursors are, among other technologies, fabricated by the dehydration of coarse gibbsite floccules at atmospheric pressure in air. In this connection, further research on the effect of thermal treatment conditions on the phase and structural transformations of gibbsite, kinetic regularities of boehmite and alumina phase formation, and phase distribution directly in the bulk of gibbsite floccules is necessary. The results of such research would allow controlling the properties of alumina carriers and catalysis thereof already at the stage of phase transitions in gibbsite.

In the present work we studied the regularities of phase formation and phase distribution in the dehydration of coarse gibbsite floccules at atmospheric pressure in air.

According to scanning electron microscopy (SEM) data (Fig. 1), synthetic gibbsite floccules are round-shaped crystalline aggregates comprising block crystals with a hexagonal profile and $\leq 10 \mu\text{m}$ in size. Elemental analysis showed that gibbsite contains SiO_2 (0.36 wt %), Na_2O (0.03 wt %), and Fe_2O_3 (0.03 wt %) admixtures.

The kinetic curves of gibbsite transformation and aluminum hydroxide and oxide phase formation are presented in Fig. 2. Comparison of thermal and X-ray phase (XPA) analysis data shows that the boehmite phase in gibbsite dehydration products can comprise,

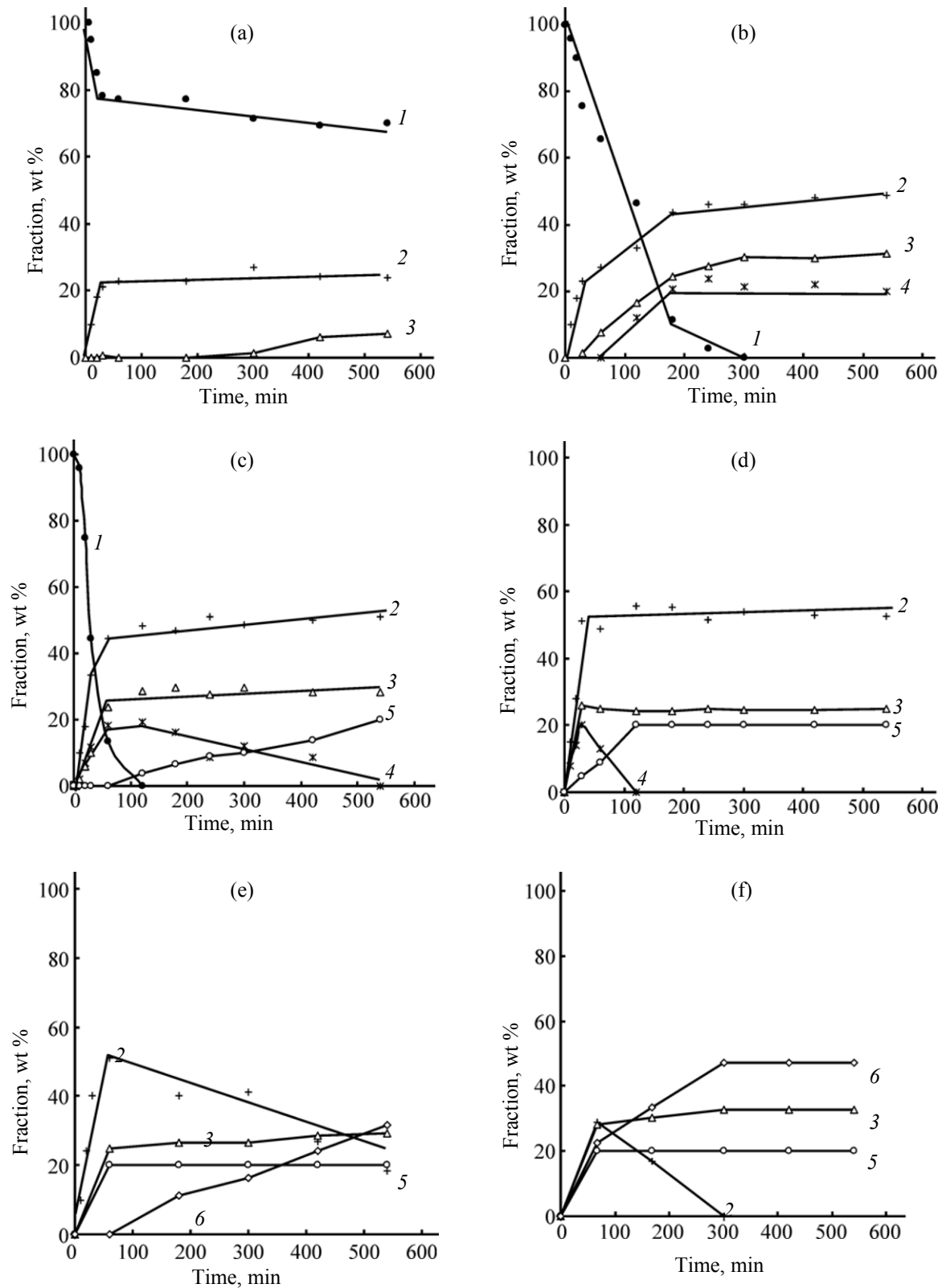


Fig. 2. Kinetic curves of gibbsite transformation and hydroxide and alumina phase formation at (a) 250, (b) 300, (c) 350, (d) 400, (e) 450, and (f) 500°C. (1) Gibbsite; (2) boehmite; (3) γ -Al₂O₃; (4) finely crystalline boehmite; (5) γ -Al₂O₃ obtained from finely crystalline boehmite; and (6) γ -Al₂O₃, obtained from coarse crystalline boehmite.

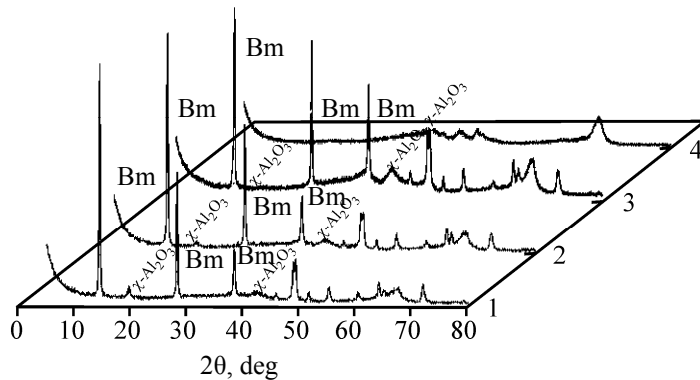


Fig. 3. X-ray diffraction patterns of gibbsite dehydration products obtained at (1) 300°C, τ 300 min, (2) 400°C, τ 300 min, (3) 450°C, τ 300 min and (4) 500°C, τ 300 min. (Bm) stands for boehmite.

depending on the treatment temperature and time, two types of differently sized particles: coarse and fine. The oxide phase can be represented by both $\chi\text{-Al}_2\text{O}_3$ and a mixture of $\chi\text{-Al}_2\text{O}_3$ and $\gamma\text{-Al}_2\text{O}_3$.

The first phase to be formed in gibbsite dehydration products is the coarsely crystalline boehmite phase. Its fraction reaches ~24 wt % at 250°C and increases to ~56 wt % at 350°C (Fig. 2), as judged from the increased weight losses in the region of the boehmite– $\gamma\text{-Al}_2\text{O}_3$ phase transition (ΔT 450–620°C, T_{\min} 546–549°C) in the DSC curves and increased boehmite line intensities in the XPA patterns of the samples (Fig. 3). The compositions calculated from the dependence of the interplanar spacing along the *b* axis on the mole fraction of water [13], coarse crystalline boehmite contains 1.02 mol of H₂O per 1 mol of Al₂O₃, and the coherent scattering regions of its crystals are, on the average, $D_{(020)}$ 50.5 and $D_{(120)}$ 40.5 nm, which is slightly smaller than the size of the starting gibbsite crystals (Table 1).

Kinetic calculations using a number of mathematical models for solid-phase reactions [18] show that the limiting stage is the stage of formation and/or growth of lamellar nuclei of coarse crystalline boehmite (Table 2), which agrees with the conclusions in [19–21]. The apparent activation energies (E_a) calculated for the stages of gibbsite decompositions and coarse crystalline boehmite formation are 74±4 and 62±4 kJ/mol, respectively. Similar values were obtained in [19], and, therewith, coarse boehmite crystals are formed exclusively from coarse gibbsite crystals.

The formation of up to 24 wt % of a finely crystalline boehmite (Fig. 2) is indirectly evidenced by

the appearance in the DSC curves of an additional well-defined endotherm at ~320–460°C with its minimum at 418–426°C. The E_a for the finely crystalline boehmite is higher compared to that for coarse crystalline boehmite and comprises 94±7 kJ/mol (Table 2). There are different explanations in the literature for the two endothermic effects in the DSC–DTG curves for the boehmite– $\gamma\text{-Al}_2\text{O}_3$ phase transitions. Panasyuk et al. [27] studied the boehmite dehydration (T_{\min} 365–371°C) and decomposition stages (T_{\min} 510–513°C). Alex et al. [28] interpreted the two effects (T_{\min} 427 and 527°C) in the DTG curve of boehmite subjected to mechanochemical activation by stepwise dehydroxylation of Al–OH–Al and Al–OH groups in the structure-forming octahedra. Analysis of a broad range of samples revealed only one effect from the $\gamma\text{-AlOOH}\cdot n\text{H}_2\text{O} \rightarrow \gamma\text{-Al}_2\text{O}_3$ phase transition either at a low temperature, like in the dehydration of pseudoboehmite in [29], or at a high temperature, like in the dehydration of boehmite in the present work. The low-temperature endothermic effect in the DSK curves is most frequently observed for the phase transition to $\gamma\text{-Al}_2\text{O}_3$ of pseudoboehmite with the crystal dimensions $D_{(020)}$ 0.6–9.3 nm [29–31] or of bohemite gel [13].

Comparison of thermal and XPS analysis data allows us the assignment of the observed effect to the phase transition to $\gamma\text{-Al}_2\text{O}_3$ of boehmite particles of a smaller size than in the coarse crystalline sample. The broadening of the boehmite signals in the X-ray diffraction patterns and the fact that they have the same positions at the same 2θ angles (Fig. 3, curves 2 and 3) suggest the same quantities of structural water in both boehmites. According to calculations, the coherent scattering range of boehmite particles comprising both the coarse crystalline and finely

Table 1. Effect of the conditions of gibbsite thermal treatment on the coherent scattering ranges (nm) of boehmite crystals and the composition of the boehmite phase

Treatment conditions		Gibbsite		Mixture of coarsely and finely crystalline boehmite phases		Calculated for finely crystalline boehmite ^a		Composition of the boehmite phase, wt %	
								coarse crystalline boehmite	finely crystalline boehmite
T, °C	τ, min	D ₍₀₀₂₎	D ₍₁₁₀₎	D ₍₀₂₀₎	D ₍₁₂₀₎	D ₋₍₀₂₀₎	D ₋₍₁₂₀₎		
Starting gibbsite		67.5	55.0	—	—	—	—	—	—
250	60	65.8	57.0	50.2	38.6	—	—	100	—
	180	58.5	55.0	51.3	40.4	—	—	100	—
	300	57.6	55.0	50.2	42.3	—	—	100	—
	540	54.8	55.0	48.5	40.6	—	—	100	—
300	180	36.2	30.0	37.8	36.8	11.8	28.9	68.1	31.9
	240	34.0	29.9	36.7	34.9	10.9	23.9	66.4	33.9
	300	—	—	39.7	35.5	17.4	24.7	68.4	31.6
350	60	30.3	27.2	37.6	36.2	7.2	25.8	70.9	29.1
	180	—	—	38.0	33.0	5.1	12.8	73.3	25.7
	300	—	—	40.0	34.7	2.0	12.3	79.4	20.6
400	60	—	—	40.0	34.0	2.4	9.7	78.9	21.1
	180	—	—	41.6	40.4	—	—	100	—
	300	—	—	46.0	42.5	—	—	100	—
	540	—	—	39.2	40.6	—	—	100	—
450	300	—	—	36.4	40.6	—	—	76.9 ^b	—
500	180	—	—	41.6	41.2	—	—	31.0 ^b	—

^a Averaged boehmite particle size was used in the calculations. ^b The decreased concentration of boehmite is explained by its dehydration to γ-Al₂O₃.

crystalline phases decrease to D₍₀₂₀₎ 36.7–38.0 and D₍₁₂₀₎ 34.9–36.8 nm (Table 1). Therewith, the coherent scattering range of finely crystalline boehmite particles, which we calculated based on the contribution of each of the formed Boehmites to the coherent scattering range during phase accumulation at T_{ann} 300–350°C, are D₍₀₂₀₎ 7.2–17.4 and D₍₁₂₀₎ 23.9–28.9 nm. The same amounts of structural water in both Boehmites and the common mechanism of crystal nucleation and growth (Table 2) show that the Boehmites are identical in nature but have different coherent scattering ranges.

In the IR spectra the phase transition of gibbsite to coarse crystalline boehmite is accompanied by an attenuation of all absorption bands in the ranges of stretching [ν(O–H) 3624, 3528, 3471, 3393, 3375 cm⁻¹] and bending [δ(OH) 1020, 966, 915 cm⁻¹] vibrations of OH groups and vibrations of the Al_{VI}–O bonds (ν 799, 745, 667 cm⁻¹) [31–35], as well as by an appearance of new well-defined bands due to stretching [ν_s(O–H) 3292, ν_{as}(O–H) 3093 cm⁻¹] and bending [δ_{as}(OH) 1150, δ_s(OH) 1070 cm⁻¹] vibrations of the OH groups in the boehmite structure [36–38] (Fig. 4). The analysis of the spectra in the region of OH stretching vibrations

shows that the fragmentation of gibbsite particles [1] does not have any effect of the coherent scattering range of gibbsite crystals. The fragmentation of gibbsite particles is evidenced by a much stronger reduction of interlayer OH groups between gibbsite stacks [$\nu(\text{O}-\text{H}) 3528 \text{ cm}^{-1}$] compared to terminal OH groups on the (001) crystal plane [$\nu(\text{OH}) 3624 \text{ cm}^{-1}$], and intralayer OH groups both on crystal sides [$\nu(\text{OH}) 3471 \text{ cm}^{-1}$] and directly in the gibbsite stack plane [$\nu(\text{OH}) 3393, 3375 \text{ cm}^{-1}$]. The fragmentation of gibbsite particles can be favored by a much lower energy of the hydrogen bonds between interlayer OH groups compared to the hydrogen bonds between intralayer OH groups [35]. As the fraction of gibbsite decreases due to its transformation to coarsely crystalline boehmite, the $\nu(\text{O}-\text{H})$ band at 3528 cm^{-1} is attenuated more than 2 times stronger compared to the $\nu(\text{O}-\text{H})$ band at 3624 cm^{-1} and 4–8 times stronger than the $\nu(\text{O}-\text{H})$ bands at $3471, 3393$, and 3375 cm^{-1} (Fig. 5). The same results follow from a comparison of the areas of the same bands calculated by the deconvolution of IR spectral profiles into gaussian components, as well as from the residual gibbsite concentrations in the samples (Fig. 6).

At $300\text{--}350^\circ\text{C}$, when the fraction of the transformed gibbsite becomes close to 100% and the fraction of crystalline boehmite to a maximum ($\sim 56 \text{ wt } \%$), an anomalously strong growth of the split band at $3393, 3375 \text{ cm}^{-1}$ and stabilization of the intensity of the band at 3471 cm^{-1} , along with gradual attenuation of the bands at 3624 and 3528 cm^{-1} , are observed (Fig. 5).

Analysis of the gaussian components of the spectra shows that the dehydration of gibbsite is accompanied by decreasing number of intralayer OH groups in its structure, as evidenced by decreasing area of the corresponding band. The simultaneous increase of the band area at 3471 cm^{-1} , associated with increasing number of OH groups on the sides of gibbsite crystals, can be attributed to a fragmentation of the rest of gibbsite crystals because the increasing temperature causes a considerable increase in the partial pressure of water vapors inside floccules. The fragmentation phenomenon is confirmed by a considerable (1.8–2.3 times) decrease in the coherent scattering ranges of gibbsite crystals to $30.2\text{--}34.0 \text{ nm}$ along the (002) plane and to $27.2\text{--}29.9 \text{ nm}$ along the (110) plane (Table 1), which, in their turn, correlate with the band area at 3471 cm^{-1} in the IR spectra of the samples (Fig. 7).

Table 2. Kinetic characteristics of different reactions involved in the thermal decomposition of gibbsite (Avrami–Erofeev–Kolmogorov function [18])

$T, ^\circ\text{C}$	k, s^{-1}	n	R^2	$E_a, \text{kJ/mol}$
Dehydration of gibbsite				
200	6.2×10^{-6}	1.5	0.8807	74 ± 4
250	2.2×10^{-4}	1.5	0.9903	
300	2.4×10^{-4}	1.5	0.9938	
350	4.1×10^{-4}	2.0	0.9698	
Formation of coarse crystalline boehmite				
200	6.2×10^{-6}	1.5	0.8807	62 ± 4
250	1.4×10^{-4}	1.5	0.9695	
300	2.2×10^{-4}	1.5	0.9387	
350	3.0×10^{-4}	1.5	0.9937	
400	5.8×10^{-4}	2.0	0.9478	
Formation of finely crystalline boehmite				
300	5.0×10^{-5}	1.5	0.9581	94 ± 7
350	1.4×10^{-4}	1.5	0.9961	
400	3.7×10^{-4}	2.0	0.9996	
Formation of Al_2O_3				
250	8.5×10^{-6}	2.0	0.9430	86 ± 6
300	3.5×10^{-5}	2.0	0.9370	
350	7.3×10^{-5}	2.0	0.9175	
400	1.6×10^{-4}	1.5	0.9324	
450	2.1×10^{-4}	1.5	0.9666	
500	4.8×10^{-4}	2.0	0.9467	

Apparently, the fragmentation products are precursors of the finely crystalline boehmite phase. The decrease of the coherent scattering range of gibbsite and increase of the band area at 3471 cm^{-1} in the IR spectra coincide with the appearance of this phase at 300°C (Fig. 1). The long induction period ($\sim 120 \text{ min}$) can be due to the slow rise to the maximum value of the pressure of water vapors in the central part of floccules in the course of the formation of coarse boehmite crystals. The subsequent fragmentation of

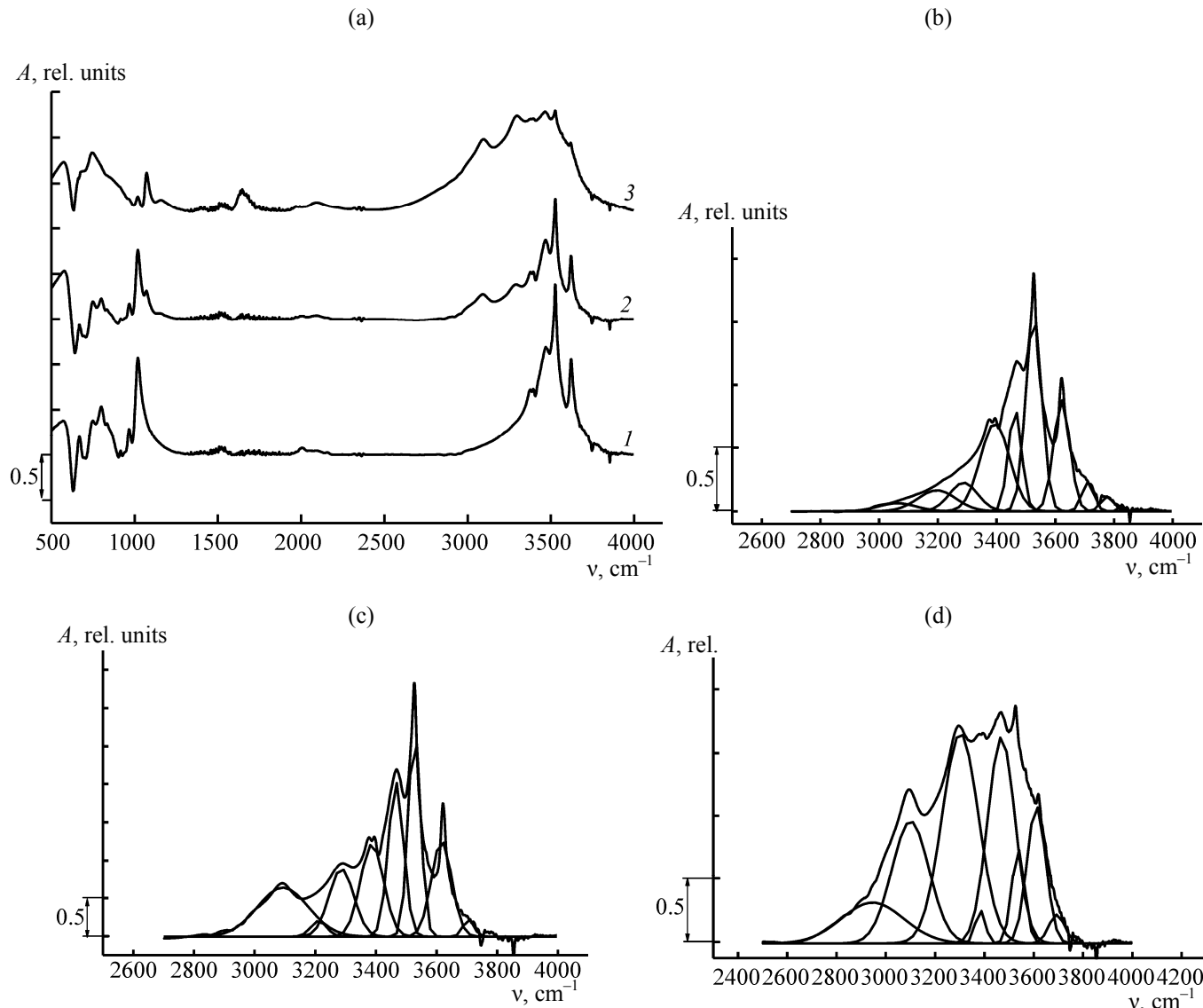


Fig. 4. (a) IR spectra and gaussian deconvoluted fragments of the IR spectra of (1, b) the starting gibbsite and its thermal treatment products obtained at (2, c) 250°C, τ 300 min and (3, d) 350°C, τ 60 min.

gibbsite crystals because of the fast release of water vapors to the environment is accompanied by a development of an open-pore system, as evidenced by a considerable increase of the specific surface area of the dehydration products (from 0.7 to 96.3 m²/g). The fragmented gibbsite crystals, primarily in the central part of floccules, undergo dehydration to form finely crystalline boehmite (Fig. 1). The latter conclusion follows from the analysis of the dispersed (0.2–3.0 μ m) particles of gibbsite dehydration products, chipped from the surface of floccules.

The dispersed particles of the dehydration products obtained at 300°C (540 min) and 350°C (240 min)

contain almost 2 times less finely crystalline boehmite than the starting floccules (Table 3). Consequently, this phase is best formed in the central phase of floccules. Therewith, initially, at 250°C the coarse crystalline boehmite phase is formed in the entire floccule bulk, and at 300–350°C finely crystalline boehmite nuclei are formed in the floccule center.

Unlike finely crystalline boehmite, the γ -Al₂O₃ phase mostly crystallizes on the outer surface of gibbsite floccules, which contacts with the environment (atmospheric air), or on the surface of pores already after gibbsite crystals have fragmented [1, 21], i.e. in those regions, where water vapors are

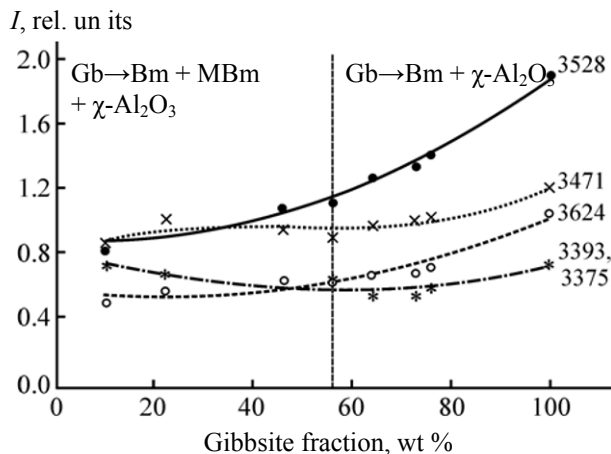


Fig. 5. Effect of gibbsite concentration on IR band intensities. Here and hereinafter, Gb stands for gibbsite, Bm for boehmite, and MBm for finely crystalline boehmite.

able to release from the inside. Dispersed particles of all the samples in study are enriched with the $\chi\text{-Al}_2\text{O}_3$ phase whose fraction is ~4.5 times larger than in the samples obtained at 250°C and 1.4–1.6 times larger than in the samples obtained at 300–400°C (Table 3).

The $\chi\text{-Al}_2\text{O}_3$ phase not contaminated with the $\gamma\text{-Al}_2\text{O}_3$ phase is only identified in the samples obtained at 250 and 300°C, and it crystallizes with induction periods of ~300 min in the first case and ~60 min in the second case (Fig. 1), which is associated with gradual formation of an open-pore system (V_{BET} 0.03–0.20 cm³/g, S_{BET} 45.6–260.9 m²/g). In going from 250 to 300°C, the fraction of $\chi\text{-Al}_2\text{O}_3$ in the dehydration products increases from 8 to 32 wt % and then stabilizes at 350–500°C. The coherent scattering range of the forming $\chi\text{-Al}_2\text{O}_3$ crystals is $D_{(440)}$ 5.0 and $D_{(004)}$ 32.1 nm (Table 4). The long induction period and slow (k 8.5×10^{-6} – 3.5×10^{-5} s⁻¹, Table 2) crystallization of the $\chi\text{-Al}_2\text{O}_3$ phase provide evidence that the physico-chemical process of oxide formation is complicated in nature [16]. For necessary structural changes in gibbsite with subsequent formation and 2D growth of laminar nuclei of the $\chi\text{-Al}_2\text{O}_3$ phase a long time is required. According to calculations (Table 2), the exponent in the Avrami–Erofeev–Kolmogorov equation is equal to 2.0.

Thus, in the floccules of gibbsite dehydration products, including the $\chi\text{-Al}_2\text{O}_3$ phase, a finely crystalline boehmite core surrounded by a coarse crystalline boehmite layer is formed. Both the boehmite phases are coated, on the outer surface of floccules, by a $\chi\text{-Al}_2\text{O}_3$ layer which is partly distributed in the bulk of floccules along the walls of open pores.

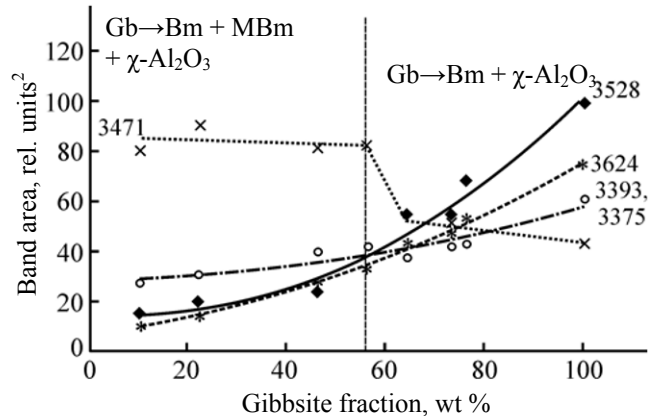


Fig. 6. Effect of gibbsite concentration on the band areas in the IR spectra deconvolved into gaussian components.

When the calcination temperature of gibbsite is increased to 500°C, the oxide fraction in the dehydration products increases due to the $\gamma\text{-Al}_2\text{O}_3$ phase formed by dehydration not only of finely crystalline (350–400°C), but also of coarse crystalline (450–500°C) boehmite (Fig. 1). The dehydration of finely crystalline boehmite is complete at 400°C after ~120 min, and the dehydration of coarsely crystalline boehmite at 500°C is complete after ~300 min (Fig. 3, pattern 4).

The kinetic curves of the formation of the alumina phase comprising $\chi\text{-Al}_2\text{O}_3$ and $\gamma\text{-Al}_2\text{O}_3$ are described, like in the previous cases, by the Avrami–Erofeev–Kolmogorov equation with the exponent n 1.5–2.0.

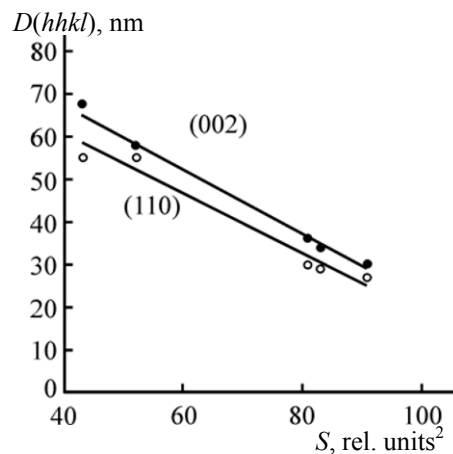


Fig. 7. Plot of the coherent scattering range of gibbsite crystals vs areas of the $v(\text{O}-\text{H})$ bands at 3471 cm^{-1} in the IR spectra.

Table 3. Phase compositions (wt %) of floccules and dispersed particles obtained by fluidized-bed abrasion

Phase	250°C, 540 min		300°C, 540 min		350°C, 240 min		400°C, 540 min	
	starting floccules	dispersed particles						
Gibbsite	65.0	33.9	—	—	—	—	—	—
Coarse crystalline boehmite	29.0	30.0	48.8	42.5	51.0	45.8	52.9	44.0
Finely crystalline boehmite	—	—	20.0	9.5	8.7	4.2	—	—
$\chi\text{-Al}_2\text{O}_3$	8.0	36.1	28.1	44.9	27.5	37.2	24.3	33.2
$\gamma\text{-Al}_2\text{O}_3$	—	—	3.1	3.1	12.8	12.8	22.8	22.8

Table 4. Effect of the conditions of gibbsite thermal treatment on the coherent scattering ranges (nm) of Al_2O_3 crystals and the composition of the alumina phase

Treatment conditions		Mixture of $\chi\text{-Al}_2\text{O}_3$ and $\gamma\text{-Al}_2\text{O}_3$		Calculated for $\gamma\text{-Al}_2\text{O}_3$		Alumina fraction in the sample, wt %	
T, °C	τ , min	$D_{(440)}$	$D_{(004)}$	$D_{(440)}$	$D_{(004)}$	$\chi\text{-Al}_2\text{O}_3$	$\gamma\text{-Al}_2\text{O}_3$
250	540	—	—	—	—	8.0	—
300	300	15.0	32.1	—	—	30.6	—
350	180	13.0	28.5	2.5	9.4	30.5	6.4
	300	12.5	27.9	2.9	8.5	29.5	9.4
400	60	12.7	26.7	2.7	8.1	29.0	9.0
	300	11.3	24.1	3.7	7.7	24.6	21.4
	540	11.1	24.1	3.9	9.6	24.8	22.8
450	300	9.3	18.1	3.0	2.5	26.5	32.3
	540	7.7	14.0	3.2	3.0	29.9	51.8
500	180	8.1	14.3	4.0	3.8	30.2	53.2
	300	6.4	11.6	2.4	2.5	32.7	67.3

Consequently, the rate of the solid-phase reaction is controlled by the formation and growth of laminar $\gamma\text{-Al}_2\text{O}_3$ nuclei. The apparent activation energy of alumina phase formation is 86 ± 6 kJ/mol. Therewith, initially $\gamma\text{-Al}_2\text{O}_3$ crystals are formed, which are much smaller compared to $\chi\text{-Al}_2\text{O}_3$ crystals (Table 4). The crystal dimensions of $\gamma\text{-Al}_2\text{O}_3$ resulting from the dehydration of finely crystalline boehmite at 350–400°C [Figs. 2c, 2d], calculated with accounting for the contributions of $\chi\text{-Al}_2\text{O}_3$ and $\gamma\text{-Al}_2\text{O}_3$ to the coherent scattering range, are $D_{(440)} 2.5\text{--}3.9$ and $D_{(004)} 7.7\text{--}9.6$ nm. After coarse crystalline boehmite has undergone dehydration at 450–500°C to form $\gamma\text{-Al}_2\text{O}_3$ (Figs. 2e, 2f), the crystals no longer virtually change size along

the (440) plane (2.4–4.0 nm) but become more than 2 times shorter along the (004) plane (2.5–3.8 nm).

The dehydration products obtained at 350–400°C are mixed-phase particles consisting of a finely crystalline boehmite and/or $\gamma\text{-Al}_2\text{O}_3$ core, its surrounding layer of coarse crystalline boehmite, and the peripheral layer of laminar $\chi\text{-Al}_2\text{O}$ crystals. In the dehydration products obtained at 450–500°C, the particle core consists of finely crystalline boehmite and $\gamma\text{-Al}_2\text{O}_3$, a layer of coarse crystalline boehmite and/or $\gamma\text{-Al}_2\text{O}_3$, and an outer $\chi\text{-Al}_2\text{O}_3$ layer. The mixed-phase particles are similar in habitus to the starting gibbsite crystals, which, in its turn, predetermine floccule shape

retention, and, therewith, the surface of the particles has large fractures and cracks (Fig. 1).

Our research on the influence of the conditions of thermal treatment of floccules on the phase composition and kinetic regularities of hydroxide and alumina phase formation allows the following conclusions. Thermal treatment of gibbsite floccules in air at 250–500°C gives rise to solid-phase transformation in the dehydration products to form new phases, specifically, coarse crystalline and finely crystalline boehmites and predominantly laminar aluminas (χ -Al₂O₃, γ -Al₂O₃); the limiting stage is the formation and/or growth of nuclei of a new phase. In the 250–300°C range, a core of finely crystalline boehmite is formed in the bulk of the decomposing gibbsite floccules. This process starts with an induction period, during which partial fragmentation of gibbsite crystals because of an increase of the partial pressure of water vapors takes place. A layer of coarse boehmite crystals surrounds the finely crystalline boehmite core. χ -Al₂O₃ predominantly crystallizes on the outer surface of gibbsite particles that contacts with the environment. The mixed-phase particles obtained at 350–400°C consist of a core of fine boehmite and/or γ -Al₂O₃ crystals, which is surrounded by a layer of laminar crystals of unreacted coarse boehmite and/or γ -Al₂O₃ crystals. The outer, peripheral particle layer is composed of laminar χ -Al₂O₃ crystals.

EXPERIMENTAL

Gibbsite of GD00 brand (Bogoslovsk aluminum plant, Russia) was used as the starting material. Phase transitions that occur under heating from 250 to 500°C were studied using 40–180 µm floccules, heating was performed at a rate of 5 deg/min in air for 10–540 min.

The elemental composition of the catalyst was determined by X-ray fluorescence spectroscopy on a Clever C31 instrument (ELERAN, Russia).

Scanning electron microscopy was performed on an EVO 50 XVP electron microscope hyphenated with an INCA 350 energy dispersive spectrometer. The energy resolution of the spectrometer was 130 eV, accelerating voltage 20 keV, working distance 8 mm.

Thermal analysis was performed on a Netzsch STA-449C Jupiter combined TG+DTA analyser hyphenated with a QMS 403 D Aëlos quadrupole mass spectrometer, heating range 30–1000°C, heating rate 10 deg/min, argon atmosphere.

Phase analysis was performed on a Shimadzu XRD-7000 diffractometer (CuK_α radiation, graphite monochromator), the 2θ angle was varied from 5° to 90° with steps of 0.05°. Phases were identified by their characteristic diffraction lines: γ -Al(OH)₃ (ICSD no. 200599), γ -AlOOH (ICSD no. 6162), γ -Al₂O₃ (ICSD no. 66559), and χ -Al₂O₃ (ICSD no. 13-373). The coherent scattering ranges were calculated by the Selyakov–Sherer formula to an accuracy of ~10%.

The IR spectra were measured on a Bruker VERTEX 70 instrument at room temperature in KBr tablets. The spectra were measured with a resolution of 1 cm⁻¹ and averaged by 128 scans. The base line was drawn according to [39]. The deconvolution of the spectra into gaussian components and their optimization were performed using ORIGIN [39].

Dispersed particles (0.2–3.0 µm) of gibbsite dehydration products were obtained by long-time (8 h) fluidized-bed abrasion of the surface of floccules under a stream of air.

Particle dimensions were determined on a Malvern Mastersizer 2000 laser diffraction particle size analyzer, measurement range 0.1–1000 µm.

ACKNOWLEDGMENTS

The authors express their gratitude to A.V. Gerasimov [Federal Center for Joint Use, Kazan (Volga) Federal University] for performing thermal analysis.

The work was financially supported by the Ministry of Education and Science of the Russian Federation (project no. 02.G25.31.0053).

REFERENCES

1. De Boer, J.H., Van den Heuvel, A., and Lansen, B.G., *J. Catal.*, 1964, vol. 3, no. 3, p. 268. DOI: 10.1016/0021-9517(64)90173-3.
2. Ismagilov, Z.R., Shkrabina, R.A., and Koryabkina, N.A., *Alyumoksidnye nositeli: proizvodstvo, svoistva i primenie v kataliticheskikh processakh zashchity okruzhayushchei sredy: Analiticheskii obzor* (Aluminium Supports: Production, Properties, and Applications in Catalytic Processes of Environmental Protection: Analytical Review), Novosibirsk: Institut kataliza im. G.K. Boreskova, 1998.
3. Pinakov, V.I., Stoyanskii, O.I., Tanashev, Yu.Yu., Pikkarevskii, A.A., Grinbergi B.E., Dryab, V.N., Kulik, K.V., Danilevich, V.V., Kuznetsov, D.V., and Parmon, V.N., *Katal. Prom-sti*, 2004, Special issue, p. 55.

4. Pinakov, V.I., Stoyanovsky, O.I., Tanashev, Yu.Yu., Pikkarevsky, A.A., Grinberg, B.E., Dryab, V.N., Kulik, K.V., Danilevich, V.V., Kuznetsov, D.V., and Parmon, V.N., *Chem. Eng. J.*, 2005, vol. 107, p. 157. DOI: 10.1016/j.cej.2004.12.026.
5. *Light Metals*, Lindsay, S.J., Ed., Hoboken: Wiley, 2011, p. 151.
6. Lopushan, V.I., Kuznetsov, G.F., Pletnev, R.N., and Kleshchev, D.G., *Izv. Akad. Nauk, Ser. Fiz.*, 2007, vol. 71, no. 8, p. 1222; Lopushan, V.I., Kuznetsov, G.F., Pletnev, R.N., and Kleshchev, D.G., *Bull. Russ. Acad. Sci. Phys.*, vol. 71, no. 8, p. 1187. DOI: 10.3103/S1062873807080394.
7. Pakhomov, N.A., Kashkin, V.N., Molchanov, V.V., Noskov, A.S., and Nadtochii, V.I., *Gazokhimiya*, 2008, no. 4, p. 669.
8. Gil'manov, H.H., Nesterov, O.N., Lamberov, A.A., Bekmukhamedov, G.Je., Kataev, A.N., and Egorova, S.R., *Katal. Prom-sti*, 2010, no. 1, p. 53.
9. Whittington, B. and Ilievski, D., *Chem. Eng. J.*, 2004, vol. 98, nos. 1–2, p. 89. DOI: 10.1016/S1385-8947(03)00207-9.
10. Lamberov, A.A. and Gil'manov, H.H., *Modernizatsiya katalizatorov i tekhnologii sinteza izoprena na OAO* (Modernization of Catalysts and Technologies of Isoprene Synthesis at "Nizhnekamsk-Neftekhim" OAO), Kazan: Kazan. Univ., 2012.
11. Zolotovskii, B.P., Paramzin, S.M., and Buyanov, R.A., *Kinet. Katal.*, 1990, vol. 31, no. 3, p. 751.
12. Kleshchev, D.G., Shenkman, A.I., and Pletnev, R.N., *Vliyanie sredy na fazovye i khimicheskie prevrashcheniya v dispersnykh sistemakh* (Effect of the Medium on the Phase and Chemical Transformations in Dispersed Systems), Sverdlovsk: Ural Otd. Akad. Nauk SSSR, 1990.
13. *Physical and Chemical Aspects of Adsorbents and Catalysts*, Linsen, B.G., Ed., New York: Academic, 1970.
14. Chukin, G.D. and Seleznev, Yu.L., *Kinet. Katal.*, 1989, vol. 30, no. 1, p. 69.
15. Serena, S., Raso, M.A., Rodriguez, M.A., Caballero, A., and Leo, T.J., *Ceram. Int.*, 2009, vol. 35, p. 3081. DOI: 10.1016/j.ceramint.2009.04.014.
16. Kogure, T., *J. Am. Ceram. Soc.*, 1999, vol. 82, no. 3, p. 716. DOI: 10.1111/j.1151-2916.1999.tb01822.x.
17. Paramzin, S.M., Zolotovskii, B.N., Buyanov, R.Ya., and Krivoruchko, O.P., *Sib. Khim. Zh.*, 1992, no. 2, p. 130.
18. Brown, M., Dollimore, D., and Galwey, A.K., *Comprehensive Chemical Kinetics*, Bamford, C.H. and Tipper, T.F.H., Eds., Amsterdam: Elsevier, 1980, vol. 22, p. 1.
19. Madarasz, J., Pocol, G., Novak, C., Tamatit Cobos, F., and Gal, S., *J. Thermal Anal.*, 1992, vol. 38, p. 445. DOI: 10.1007/BF01915509.
20. Peric, J., Krstulovic, R., and Vucak, M., *J. Thermal Anal.*, 1996, vol. 46, p. 1339. DOI: 10.1007/BF01979247.
21. Candela, L. and Perlmutter, D.D., *Ind. Eng. Chem. Res.*, 1992, vol. 31, p. 694. DOI: 10.1021/ie00003a007.
22. Stacey, M.H., *Langmuir*, 1987, vol. 3, no. 5, p. 681. DOI: 10.1021/la00077a018.
23. Wang, H., Xu, B., Smith, P., Davies, M., DeSilva, L., and Wingate, C., *J. Phys. Chem. Solids*, 2006, vol. 67, p. 2567. DOI: 10.1016/j.jpcs.2006.07.016.
24. Pakhomov, N.A., *Promyshl. Katal. Lekts.*, 2006, no. 6, p. 53.
25. Flid, M.R. and Treger, Yu.A., *Vinilkhlorid: khimiya i tekhnologiya* (Vinyl Chloride: Chemistry and Technology), Moscow: Kalvis, 2008, book 1.
26. Lainer, A.I., Eremin, N.I., Lainer, Yu.A., and Pevzner, I.Z., *Proizvodstvo glinozemata* (Production of Alumina), Moscow: Metallurgiya, 1978.
27. Panasyuk, G.P., Belan, V.N., Voroshilov, I.L., and Kozerozhets, I.V., *Neorg. Mater.*, 2010, vol. 46, no. 7, p. 831.
28. Alex, T.C., Kumar, C.S., Kailath, A.J., Kumar, R., and Roy, S.K., *Metall. Mater. Trans.*, 2011, vol. B42, p. 592.
29. Ivanova, A.S., Litvak, G.S., Kryukova, G.N., Tsybulya, S.V., and Paukshtis, E.A., *Kinet. Katal.*, 2000, vol. 41, no. 1, p. 137.
30. Aptikasheva, A.G., Lamberov, A.A., Egorova, S.R., Levin, O.V., and Gil'manov, H.H., *Russ. J. Phys. Chem. A*, 2005, vol. 79, no. 10, p. 1633.
31. Ingram-Jones, V.J., Slade, R.C.T., Davies, T.W., Southern, J.C., and Salvador, S., *J. Mater. Chem.*, 1996, vol. 6, no. 1, p. 73.
32. Phambu, N., Humbert, B., and Burneau, A., *Langmuir*, 2000, vol. 16, p. 6200.
33. Kloprogge, J.T., Ruan, H.D., and Frost, R.L., *J. Mater. Sci.*, 2002, vol. 37, p. 1121.
34. Desset, S., Spalla, O., Lixon, P., and Cabane, B., *Colloid Surf. A*, 2002, vol. 196, p. 1.
35. Mardilovich, P.P. and Trokhimets, A.I., *Zh. Prikl. Spektrosk.*, 1980, vol. 36, no. 2, p. 258.
36. Boumaza, A., Favaro, L., Ledion, J., Sattonnay, G., Brubach, J.B., Berthet, P., Huntz, A.M., Roy, P., and Tetot, R., *J. Solid State Chem.*, 2009, vol. 182, p. 1171.
37. Krishna Priya, G., Padmaja, P., Warrier, K.G., Damodaran, A.D., and Aruldas, G., *J. Mater. Sci. Lett.*, 1997, vol. 16, p. 1584.
38. Ram, S., *Infrared Phys. Technol.*, 2001, vol. 42, p. 547.
39. Paukshtis, E.A., *Opticheskaya spektroskopiya v adsorbtsii i katalize. Primenenie IK spektroskopii* (Optical Spectroscopy in Adsorption and Catalysis. Application of IR Spectroscopy), Novosibirsk: Inst. Katal. Sib. Otd. Ross. Akad. Nauk, 2010.